

Generality of shear thickening in dense suspensions

Eric Brown^{1*}, Nicole A. Forman^{2,3}, Carlos S. Orellana¹, Hanjun Zhang³, Benjamin W. Maynor², Douglas E. Betts³, Joseph M. DeSimone^{2,3} and Heinrich M. Jaeger¹

Suspensions are of wide interest and form the basis for many smart fluids^{1–7}. For most suspensions, the viscosity decreases with increasing shear rate, that is, they shear thin. Few are reported to do the opposite, that is, shear thicken, despite the longstanding expectation that shear thickening is a generic type of suspension behaviour^{8,9}. Here we resolve this apparent contradiction. We demonstrate that shear thickening can be masked by a yield stress and can be recovered when the yield stress is decreased below a threshold. We show the generality of this argument and quantify the threshold in rheology experiments where we control yield stresses arising from a variety of sources, such as attractions from particle surface interactions, induced dipoles from applied electric and magnetic fields, as well as confinement of hard particles at high packing fractions. These findings open up possibilities for the design of smart suspensions that combine shear thickening with electro- or magnetorheological response.

Shear thickening is presumed to be due to general mechanisms such as hydrodynamics^{9,10} or dilation^{11–13}, and thus all suspensions are expected to show shear thickening under the right conditions⁸. So far, however, the exact conditions have not been determined. One condition is apparently set by attractive particle interactions. It has long been known that attractions, observed as flocculation in suspensions, can prevent shear thickening. This has been shown by modifying the chemistry, for example by adding flocculating agents to observe the transition from shear thickening to thinning (for a review, see ref. 8). In other cases, crossing the gel transition was shown to eliminate shear thickening^{14,15}. A key problem, therefore, is to understand how interparticle attractions interfere with shear thickening. We demonstrate here that a simple and direct criterion for the existence of an observable shear-thickening regime in dense, non-Brownian suspensions can be developed by comparing the yield stress produced by attractions with the inherent shear-thickening stresses. We then generalize this condition to show how a yield stress from any source modifies the shear-thickening phase diagram.

Our experiments used an Anton Paar rheometer to measure the shear stress τ and the shear rate $\dot{\gamma}$ of a wide range of different suspensions. The viscosity is defined as $\eta \equiv \tau/\dot{\gamma}$ in the steady state. Our focus is on non-Brownian, dense suspensions that show strongly packing-fraction-dependent, reversible shear thickening, often called ‘discontinuous’, because of the steep stress–shear rate relationship. To understand the significance of interparticle attractions, we first consider the particle–liquid surface tension. Figure 1 shows the striking change in behaviour produced by adding a small amount of surfactant to a water suspension of glass spheres with a hydrophobic coating. In the aqueous environment the coating leads to network-like particle clusters (Fig. 1b, top), which minimize exposed surface area and thus potential energy. As a consequence, to pull particles apart requires overcoming a

significant stress threshold. In Fig. 1 this translates into a region where, for applied stresses smaller than this yield stress, the suspension does not flow and the viscosity effectively diverges. The result is shear-thinning behaviour (Δ). Added surfactant eliminates the clustering with its associated yield stress and reveals a region of underlying shear thickening (\bullet) below the range of the previous yield stress. This suggests the yield stress resulting from attractions is responsible for hiding shear thickening if it overwhelms the shear-thickening stress range.

For a more-detailed exploration than afforded by chemical means of the role of the magnitude of the yield stress in modifying the shear-thickening regime, we require *in situ*, tunable control over the strength of the attractions. This can be achieved by applied electric and magnetic fields that polarize particles of a given dielectric or magnetic susceptibility and also have the practical advantage of reversibility. The result is a field-dependent attraction between neighbouring particles and thus a continuously tunable yield stress. We used dielectric glass spheres in mineral oil for electrorheology and magnetite-filled polyethylene glycol (PEG) rods suspended in PEG for magnetorheology. Figure 2 shows the evolution of the yield stress and shear-thickening regime with both types of field. For small fields, the viscosity curve is seemingly unaffected. A main result from these data is that increasing the field strength, and the concomitant yield stress, pushes the onset of shear thickening to higher stress values. At intermediate field values, the curves rejoin the zero-field shear-thickening behaviour after showing a viscosity minimum. A yield stress thus simply results in a smaller range of applied stresses over which shear thickening is observable. Only when the yield stress becomes large enough that it encroaches on the upper limit of the shear-thickening range is the effect fully eliminated. Qualitatively this behaviour is neither dependent on the suspension nor the source of the yield stress, as seen from the similarity between Fig. 2a and c. The fact that the same conclusion can apply to Fig. 1 is especially remarkable considering that the induced dipoles are directional but the chemical attractions are anisotropic. Given the different microstructures, this indicates that it is the stress scale resulting from attractions that determines whether shear thickening is observable or not.

The experiments discussed so far concerned yield stresses produced by particle attractions. Similar behaviour carries over to suspensions without attractive interactions in which a yield stress arises as a result of confinement at large packing fractions¹⁶. Data are shown in Fig. 3 for several different packing fractions of cornstarch in water. It is seen again that the shear-thickening range decreases as the yield stress increases and eventually disappears when this yield stress approaches the upper stress limit of the shear-thickening regime.

The interplay between yield stress and shear thickening emerging from the data in Figs 2 and 3 can be summarized in

¹James Franck Institute, The University of Chicago, Chicago, Illinois 60637, USA, ²Liquidia Technologies, Research Triangle Park, North Carolina 27709, USA, ³Department of Chemistry, University of North Carolina, Chapel Hill, North Carolina 27599, USA. *e-mail: embrown@uchicago.edu.

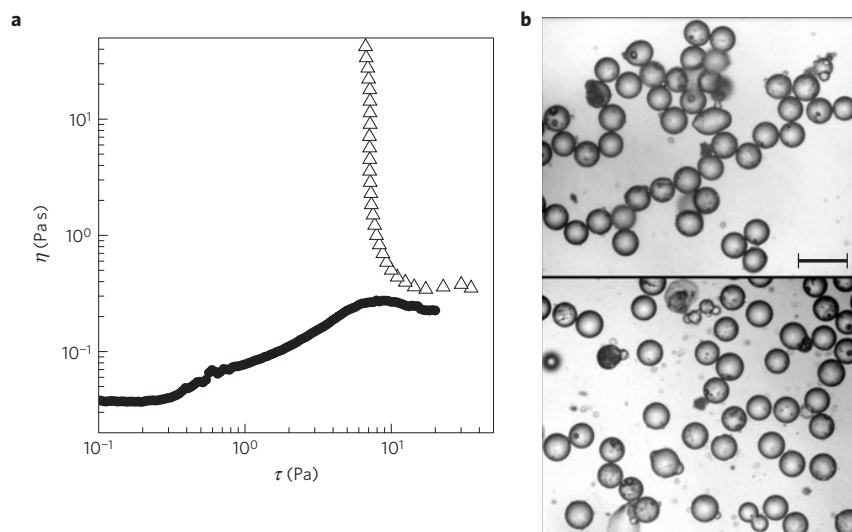


Figure 1 | Revealing shear thickening by adding surfactant to hydrophobic glass spheres in water. Soda-lime glass spheres of mean diameter 90 μm with a hydrophobic silane coating were suspended at a packing fraction $\phi = 0.52$. **a**, Triangles: viscosity curve without surfactant. The divergence of the curve is characteristic of a yield stress. Filled circles: viscosity curve of the same system at the same ϕ with added surfactant. The shear-thickening regime is the region of positive slope in the curves of viscosity η versus applied stress τ . Shear thinning is characterized by a negative slope and Newtonian fluids, such as water, show constant η . **b**, Images showing clustering as a result of interparticle attractions (top) and no clustering when surfactant is added (bottom). Scale bar: 200 μm . All images (including subsequent figures) were taken at rest under an optical microscope in a dilute quasi-two-dimensional layer. In this dilute case, attractions can be observed by the high number of particle contacts in the form of clusters or chains.

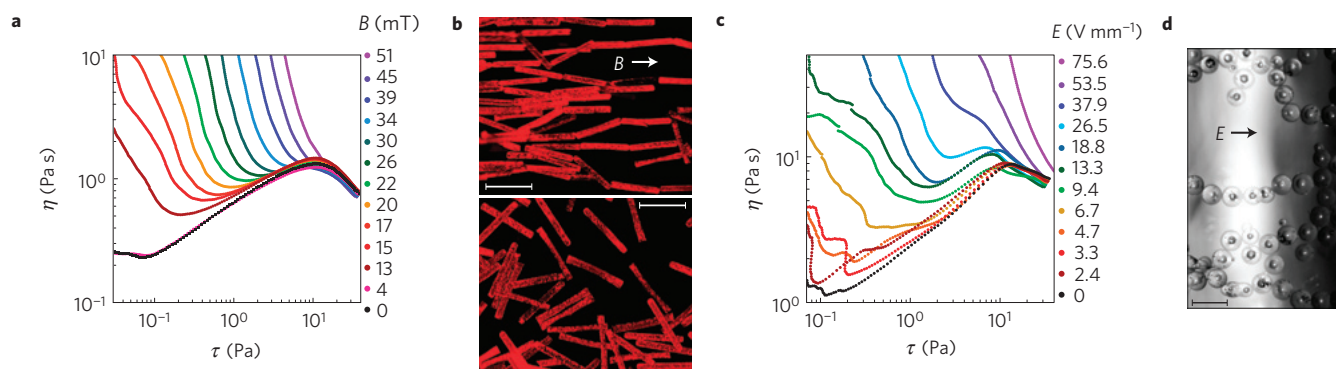


Figure 2 | Using magnetic and electric fields to tune the interplay between shear thickening and the yield stress. **a**, Viscosity curves for a suspension of ferromagnetic rods ($254 \times 32 \times 25 \mu\text{m}$) for different values of applied magnetic field B . Magnetite-doped (30% by weight) PEG rods made by the PRINT process²⁶ were suspended in PEG at a packing fraction $\phi = 0.20$. The shear-thickening region is seen to shrink and eventually becomes eliminated as it is encroached on by the increasing yield stress. **b**, Microscope images showing the rods for $B = 30 \text{ mT}$ (top) and $B = 0$ (bottom). **c**, Viscosity curves for a suspension of dielectric spheres for different values of applied electric field E . Soda-lime glass spheres of diameter 90 μm were suspended in 58 mPa s mineral oil at $\phi = 0.56$. **d**, The microscope image shows the spheres for $E = 60 \text{ V mm}^{-1}$. At $E = 0$, the image is similar to the bottom panel of Fig. 1b. In both **b** and **d** the fields were applied vertically, in the direction of the shear gradient in a parallel-plate rheometer. Scale bars: 200 μm .

a set of non-equilibrium phase diagrams (Fig. 4) showing the shear-thickening, shear-thinning and jammed (defined here as a non-flowing state below the yield stress) regimes. Despite the differences in sources of a yield stress, there are important similarities. The stress thresholds bounding this regime (horizontal black lines) are nearly independent of ϕ when the yield stress is small enough^{10,16,17}. As the yield stress increases, the lower threshold moves upward and eventually approaches the upper boundary, at which point shear thickening ceases. For intermediate values of B , E or ϕ , both jamming and shear thickening can be found at different stress values^{13,18,19}.

As the boundaries of the shear-thickening region are determined by local extrema of viscosity curves, they can be calculated given the relationship between stress and shear rate in the lower shear-thinning and shear-thickening regimes. Note that the yield stress value is below the shear-thickening phase boundary, leaving a

shear-thinning regime between the jammed and shear-thickening regions. To quantify the effect of the yield stress on the shear-thickening phase boundary, we therefore must account for this extra regime. To model these contributions, we use the Herschel–Bulkley form, with a fixed exponent of 1/2 commonly used to describe shear-thinning behaviour¹⁰.

$$\tau_{\text{HB}}(\dot{\gamma}) = \tau_y + a_1 \dot{\gamma}^{1/2} \quad (1)$$

Here the first term τ_y denotes the yield stress and a_1 parameterizes the extra stress that is operative in the shear-thinning regime. We refer to τ_{HB} as the shear-thinning stress. Earlier work^{15,20,21} suggests that contributions to the overall shear stress can be linearly separated as

$$\tau(\dot{\gamma}) = \tau_{\text{HB}}(\dot{\gamma}) + a_2 \dot{\gamma}^{1/\epsilon} \quad (2)$$

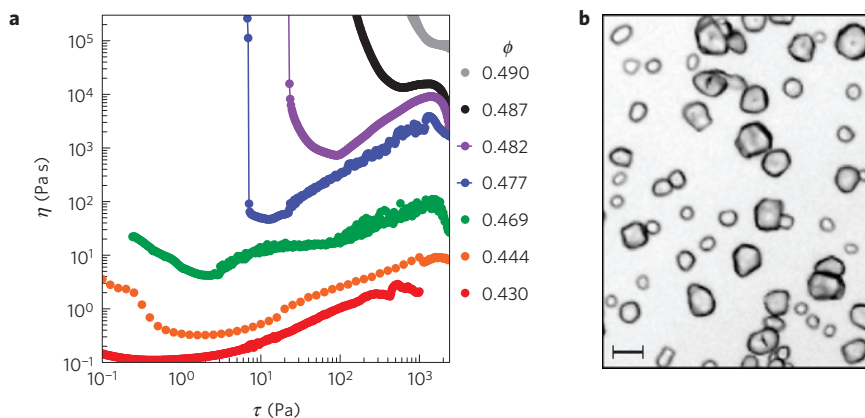


Figure 3 | Elimination of shear thickening by increasing packing fraction. **a**, Viscosity curves for cornstarch in water at different packing fractions ϕ . The cornstarch particles had an average diameter of 14 μm . The water was density-matched to 1.59 g ml^{-1} by dissolving CsCl in it. A solvent trap was used to avoid evaporation and a Couette geometry was used to ensure the sample remained confined. **b**, The microscope image shows that particles do not cluster without confinement, also confirmed by optical tweezer measurements. Scale bar: 20 μm .

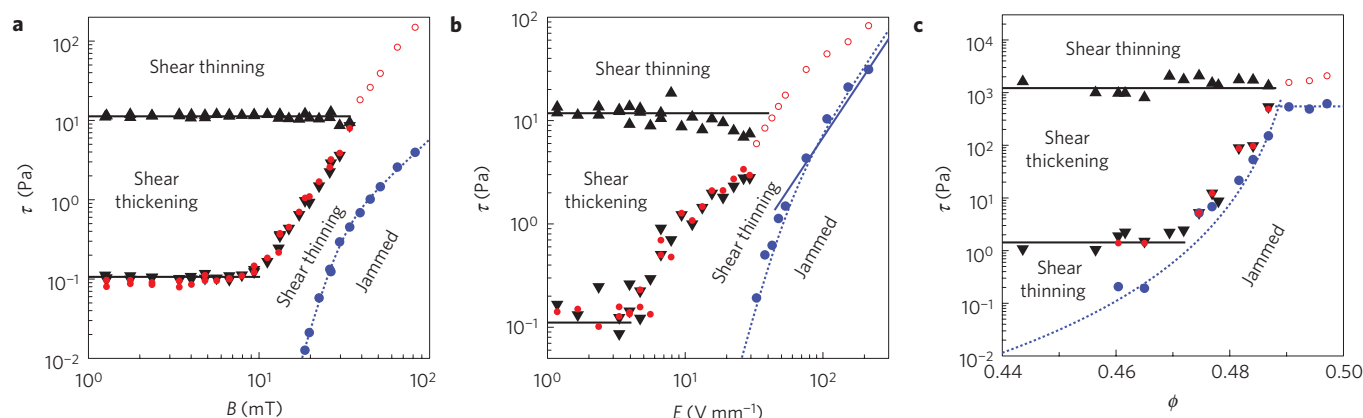


Figure 4 | Non-equilibrium phase diagrams delineating observable shear-thickening regions in terms of the associated stress range. **a–c**, Stress range as a function of applied magnetic field B (**a**), applied electric field E (**b**) and packing fraction ϕ (**c**). The boundaries of the shear-thickening regime are set by the local minima (black downtriangles) and maxima (black triangles) of the viscosity curves in Figs 2 and 3. Blue circles: the yield stress τ_y , below which suspensions are jammed. Red filled circles: the predicted onset of shear thickening τ_m evaluated from equation (3) at the measured $\dot{\gamma}_m$, demonstrating that the boundary is determined by the total shear-thinning stress τ_{HB} , regardless of the source of the yield stress. For **a** and **b**, the value of ϵ used is that measured for zero attractions, showing that the shear-thickening stress term is independent of field strength. For **c**, the value of $\epsilon = 0$ is used, which is measured at the highest packing fractions where shear thickening can be observed, showing that the phase boundary is equal to the shear-thinning stress τ_{HB} in the limit of $\epsilon = 0$. Solid black lines: the measured stresses at the upper and lower phase boundaries in the limit of zero field and small ϕ . These coincide with the measured phase boundaries for $B = 0$ and $E = 0$. Solid blue line: prediction of the electrorheological yield stress from two-particle interaction (see Supplementary Information). Dotted blue lines: guides to the eye for the phase boundary between shear-thinning and jammed regimes. Red open circles: predicted τ_m in cases where no shear-thickening regime was found using model predictions for $\dot{\gamma}_m$. In each case, these values are close to or above the upper stress boundary, showing that the reason shear thickening was not found was because τ_m exceeded the shear-thickening stress range.

where the second term represents the shear-thickening stress parameterized by a_2 and an exponent ϵ that approaches zero in the limit where the stress/shear-rate relationship becomes discontinuous at high packing fractions¹⁶. Over the whole range explored in our experiments, equation (2) fits the data well, as demonstrated by the example in Fig. 5.

The lower boundary of the shear-thickening region occurs at the stress τ_m and shear rate $\dot{\gamma}_m$ corresponding to the local viscosity minimum. Differentiating $\eta \equiv \tau/\dot{\gamma}$ and eliminating a_2 through equation (2) evaluated at τ_m gives

$$\tau_m = \tau_{\text{HB}}(\dot{\gamma}_m) + \frac{\epsilon}{2(1-\epsilon)} [\tau_{\text{HB}}(\dot{\gamma}_m) + \tau_y] \quad (3)$$

Equation (3) is in a form that directly shows how the shrinkage of the shear-thickening regime depends on the shear-thinning terms.

The model parameters ϵ , τ_y and a_1 are obtained by fitting the data to equation (2) for each value of B, E and ϕ . The values of a_2 and ϵ are found to be independent of B and E (see Supplementary Information), which can be seen from the overlay of shear-thickening curves at higher stresses in Fig. 2, indicating that the shear-thickening stress is independent of attractions. This is in contrast to weaker, ‘continuous’ shear thickening resulting from hydrodynamics where attractions were found to affect the shear-thickening stress¹⁵. Equation (3) is evaluated at the measured $\dot{\gamma}_m, \tau_y$ and a_1 for each B, E and ϕ , and a fixed value of ϵ for each panel, as shown by the filled red symbols in Fig. 4. This describes the lower phase boundary very well, typically within 12%. We note that equation (3) along with an equation for $\dot{\gamma}_m$ (obtained from equations (1) to (3), see Supplementary Information) can also be used to predict the phase boundary with attractions without measuring $\dot{\gamma}_m$ for all field values,

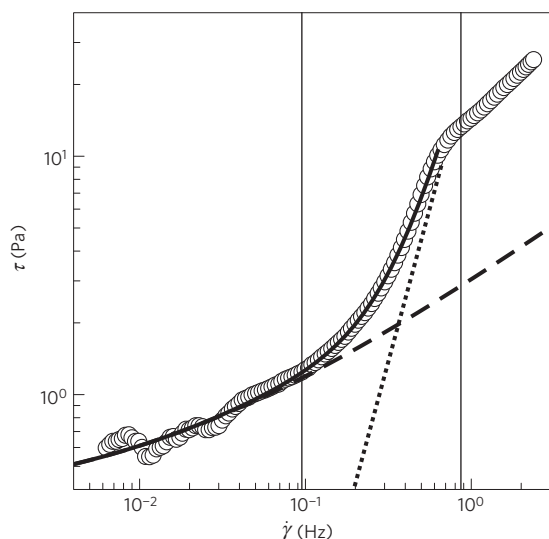


Figure 5 | Fit of a stress/shear-rate curve broken up into shear-thinning and shear-thickening components. Data shown for glass spheres at $E = 12.5 \text{ V mm}^{-1}$. Dashed line: fit of Herschel-Bulkley model (equation (1)) to the lower shear-thinning regime. Dotted line: term $\sim \dot{\gamma}^{1/\epsilon}$ representing the shear-thickening regime. Solid line: sum of the dashed and dotted lines (equation (2)). Vertical lines: shear rates corresponding to the boundaries of the shear-thickening range in the limit of $E = 0$.

assuming only that the shear-thickening stress is independent of the shear-thinning mechanism.

The agreement of equation (3) with the measured phase boundaries in Fig. 4 demonstrates that the lower shear-thickening phase boundary is set by the mechanism that produces shear thinning. As a result of the second term in equation (1), this is true whether or not the shear thinning includes a yield stress. It is also independent of whether the shear-thickening stress term is affected by the parameter that controls shear thinning if the shear-thickening and shear-thinning terms add linearly as seen in Fig. 4c and for ‘continuous’ shear thickening^{6,15}. The fact that this model reproduces the measured phase boundary confirms that, for ‘discontinuous’ shear thickening, the effect of attractions is to increase the shear-thinning stress that hides shear thickening, rather than to affect the shear-thickening stress directly. When B , E or ϕ becomes large enough that shear thickening is not observed, τ_m (open red symbols in Fig. 4) becomes higher than the shear-thickening stress range. In the limit of $\epsilon = 0$, equation (3) reduces to $\tau_m = \tau_{\text{HB}}(\dot{\gamma}_m)$, so the stress at the phase boundary becomes equal to the shear-thinning stress. Thus, the shear-thickening regime starts to shrink when the shear-thinning stress exceeds the stress at the onset of shear thickening, and it is eliminated when the shear-thinning stress exceeds the stress at the viscosity maximum. Regardless of the particulars of the mathematical model, this is a good approximation as long as there is a sharp upturn in $\tau(\dot{\gamma})$, which is the defining feature of ‘discontinuous’ shear thickening, and the shear-thickening stress term is independent of the shear-thinning mechanism. This interpretation remains true for $\epsilon > 0$ with corrections according to equation (3). It also holds in cases where there is a Newtonian regime before the onset of shear thickening, regardless of the value of ϵ (see Supplementary Information).

Our simple model predicts the shear-thickening phase boundaries without knowing detailed particle properties or microstructure. As long as the shear-thinning mechanism produces a stress term that adds linearly to the shear-thickening stress term, all sources of shear thinning have the same effect of hiding shear thickening, regardless of the mechanisms that produce shear thickening.

This description in terms of stress scales is not dependent on size scale and, in principle, might be applicable also to ‘discontinuous’ shear thickening in colloidal (that is, Brownian) systems. In colloids, however, different mechanisms for shear thickening and thinning might become relevant, for example a shear-thinning stress term resulting from Brownian motion²⁰.

The existence of an upper threshold beyond which shear-thinning mechanisms will overwhelm shear thickening explains why in most cases attractions completely eliminate shear thickening⁸ whereas for some fluids with weak interparticle attractions it has been reported to exist^{22,23}. In typical suspensions, attractions are often due to particle–fluid surface tension. An example is the common observation that cornstarch (a hydrophilic particle) shear thickens in water but not in hydrophobic liquids²⁴. One can then ask whether all suspensions will shear thicken once the shear-thinning stresses are small. In the experiments reported here on a variety of suspensions consisting of particles including cornstarch, glass and PEG, in a variety of fluids with different density matching, modified surface properties, roughness, shapes and measuring conditions, we always observed ‘discontinuous’ shear thickening. Including a variety of other suspensions we studied, we found no examples where the shear-thinning stress was small (less than the order of 5 Pa for particles of the order of 10–100 μm) that did not shear thicken at near-sedimentation packing fractions. Inductively this suggests the phenomenon of ‘discontinuous’ shear thickening is general to all hard-particle suspensions at near-sedimentation packing fractions provided that the shear-thinning stresses are below a threshold^{8,9}.

The combination of electrorheological or magnetorheological effects with shear thickening opens up possibilities for the design of field-responsive shear-thickening fluids in dampers or impact absorbers^{6,7,25}. We note that earlier suggestions presumed that the applied fields would control the critical shear rate²⁵, but this is true only for weaker shear thickening ($\epsilon > 0$), where both the critical stress and shear rate vary with field. In the limit where shear thickening becomes discontinuous ($\epsilon = 0$), our findings show that the critical shear rate is controlled by the particle packing fraction¹⁶, whereas the critical stress can be tuned either passively with particle–fluid chemistry or actively with fields.

Received 22 July 2009; accepted 30 December 2009;
published online 31 January 2010

References

- Stanway, R. Smart fluids. *Nature Sci. Tech.* **20**, 931–939.
- Wen, W., Huang, X., Yang, S., Lu, K. & Sheng, P. The giant electrorheological effect in suspensions of nanoparticles. *Nature Mater.* **2**, 727–730 (2003).
- Trappe, V., Prasad, V., Cipelletti, L., Segre, P. N. & Weitz, D. A. Jamming phase diagram for attractive particles. *Nature* **411**, 772–775 (2001).
- Jolly, M. R., Bender, J. W. & Carlson, J. D. *SPIE 5th Annual Int. Symposium on Smart Structures and Materials* (1998).
- Lee, Y. S., Wetzel, E. D. & Wagner, N. J. The ballistic impact characteristics of Kevlar—woven fabrics impregnated with a colloidal shear thickening fluid. *J. Mater. Sci.* **38**, 2825–2833 (2003).
- Shenoy, S. S., Wagner, N. J. & Bender, J. W. E-FIRST: Electric field responsive shear thickening fluids. *Rheol. Acta* **42**, 287–294 (2003).
- Zhang, X., Li, W. & Gong, X. L. Study on magnetorheological shear thickening fluid. *Smart Mater. Struct.* **17**, 015051 (2008).
- Barnes, H. A. Shear-thickening (‘Dilatancy’) in suspensions of nonaggregating solid particles dispersed in Newtonian liquids. *J. Rheol.* **33**, 329–366 (1989).
- Brady, J. F. & Bossis, G. The rheology of concentrated suspensions of spheres in simple shear flow by numerical simulation. *J. Fluid Mech.* **155**, 105–129 (1985).
- Maranzano, B. J. & Wagner, N. J. The effects of particle size on reversible shear thickening of concentrated colloidal suspensions. *J. Chem. Phys.* **114**, 10514–10527 (2001).
- Hoffmann, R. L. Discontinuous and dilatant viscosity behaviour in concentrated suspensions III. Necessary conditions for their occurrence in viscometric flows. *Adv. Colloid Interface Sci.* **17**, 161–184 (1982).
- Lootens, D., Van Damme, H., Hémar, Y. & Hébraud, P. Dilatant flow of concentrated suspensions of rough particles. *Phys. Rev. Lett.* **95**, 268302 (2005).

13. Fall, A., Huang, N., Bertrand, F., Ovarlez, G. & Bonn, D. Shear thickening of cornstarch suspensions as a reentrant jamming transition. *Phys. Rev. Lett.* **100**, 018301 (2008).
14. Galley, W. & Puddington, I. E. The hydration of starch below the gelatinization temperature. *Can. J. Res. C* **21**, 179–185 (1943).
15. Gopalakrishnan, V. & Zukoski, C. F. Effect of attractions on shear thickening in dense suspensions. *J. Rheol.* **48**, 1321–1344 (2004).
16. Brown, E. & Jaeger, H. M. Dynamic jamming point for shear thickening suspensions. *Phys. Rev. Lett.* **103**, 086001 (2009).
17. Egres, R. G. & Wagner, N. J. The rheology and microstructure of acicular precipitated calcium carbonate colloidal suspensions through the shear thickening transition. *J. Rheol.* **49**, 719–746 (2005).
18. Head, D. A., Ajdari, A. & Cates, M. E. Jamming, hysteresis, and oscillation in scalar models for shear thickening. *Phys. Rev. E* **64**, 061509 (2001).
19. Sellito, M. & Kurchan, J. Shear-thickening and entropy-driven reentrance. *Phys. Rev. Lett.* **95**, 236001 (2005).
20. Bergenholtz, J., Brady, J. F. & Vivic, M. The non-Newtonian rheology of dilute colloidal suspensions. *J. Fluid Mech.* **456**, 239–275 (2002).
21. Melrose, J. R. & Ball, R. C. Continuous shear thickening transitions in model concentrated colloids—the role of interparticle forces. *J. Rheol.* **48**, 937–960 (2004).
22. Osuji, C. O., Kim, C. & Weitz, D. A. Shear thickening and scaling of the elastic modulus in a fractal colloidal system with attractive interactions. *Phys. Rev. E* **77**, 060402 (2008).
23. Lootens, D., Van Damme, H. & Hébraud, P. Giant stress fluctuations at the jamming transition. *Phys. Rev. Lett.* **90**, 178301 (2003).
24. Pryce-Jones, J. Experiments on thixotropic and other anomalous fluids with a new rotation viscometer. *J. Sci. Instrum.* **18**, 39–48 (1941).
25. Jolly, M. R. & Bender, J. W. Field responsive shear thickening fluid. US patent 20060231357 (2001).
26. Rolland, J. P. *et al.* Direct fabrication and harvesting of monodisperse, shape-specific nanobiomaterials. *J. Am. Chem. Soc.* **127**, 10096–10100 (2005).

Acknowledgements

This work was supported by DARPA through Army grant W911NF-08-1-0209. E.B. acknowledges further support by the NSF MRSEC programme under DMR-0820054. We thank J. Xu for carrying out the optical tweezer measurements, K. Herlihy and J. Nunes for help with the magnetite-containing particle synthesis, L. Mair and R. Superfine for assistance with optical microscope images in calibrated magnetic fields and J. Sprague and M. Hunter for assistance with manufacturing of PRINT particles.

Author contributions

E.B. and H.M.J. conceived of the study and wrote the manuscript. All team members were involved in conception of manufactured particles that show both a magnetorheological and shear-thickening effect. H.Z., N.A.F., D.E.B. and J.M.D. were responsible for design and initial fabrication of these particles. N.A.F., B.W.M. and J.M.D. were responsible for production of gram quantities of these particles. E.B. and C.S.O. were responsible for the rheological measurements. E.B. analysed the data.

Additional information

The authors declare competing financial interests: details accompany the paper at www.nature.com/naturematerials. Supplementary information accompanies this paper on www.nature.com/naturematerials. Reprints and permissions information is available online at <http://npg.nature.com/reprintsandpermissions>. Correspondence and requests for materials should be addressed to E.B.